Available online at www.sciencedirect.com

ScienceDirect

journal homepage: www.elsevier.com/locate/he

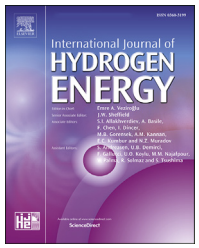

Adsorption and dissociation of H_2 molecule over first-row transition metal doped C24 nanocage as remarkable SACs: A comparative study

Sehrish Sarfaraz [a], *Muhammad Yar* [a], *Riaz Hussain* [b], *Khurshid Ayub* [a,*]

[a] *Department of Chemistry, COMSATS University, Abbottabad Campus, Abbottabad, 22060, Pakistan*
[b] *Department of Chemistry, University of Education, Campus Dera Ghazi Khan, Lahore, 32,200, Punjab, Pakistan*

HIGHLIGHTS

- First row transition metal doped C24 complexes are theoretically investigated for hydrogen dissociation reaction.
- The transition metal act as an active center for the dissociation of hydrogen molecule.
- Hydrogen dissociation is proceeded through homolytic cleavage or oxidative addition of H_2 molecule.
- Mn@C24 catalyst has the best catalytic activity with the lowest energy barrier of 0.04 eV.
- NBO and EDD analysis show the transfer of charge participated in dissociation process.

ARTICLE INFO

Article history:
Received 4 November 2022
Received in revised form
7 February 2023
Accepted 3 March 2023
Available online 21 March 2023

Keywords:
C24 nanocage
Transition metal
Hydrogen dissociation
Energy barrier
Natural bond orbital

ABSTRACT

Transition metal doped carbon materials such as carbon nanotubes and fullerenes have been extensively investigated for hydrogen adsorption and storage applications. However, the strength of these hydrogen storage material is mainly dependent on the metal-support and hydrogen-metal interaction energies. In this work, we have designed, and explored transition metal doped C24 (TM@C24) complexes as single atom catalysts for hydrogen dissociation. Adsorption energy results for all studied TM@C24 complexes reveal the high thermodynamic stability of designed TM@C24 catalysts. Among all considered TMs@C24 catalysts, the highest adsorption energy (−6.22 eV) is calculated for Mn@C24 catalyst. Moreover, H_2 dissociation mechanism is evaluated for both gas phase and in aqueous media to get insight into the solvent effect. In both gas phase and in aqueous media, the best catalytic activity for hydrogen dissociation is computed for Mn@C24 catalyst with the lowest energy barrier of 0.04 eV and 0.30 eV, respectively. NCI analysis is carried out to confirm the shared shell interactions (covalent interactions) between adsorbed hydrogen and TM@C24 complexes. Furthermore, natural bond orbital and electron density differences analysis are also performed to explore the activation and dissociation of H_2 molecule. Overall results reveal that Mn@C24 complex can at as a promising low cost, highly abundant and noble metal free single atom catalyst to effectively catalyze hydrogen dissociation reaction.

* *Corresponding author.*
E-mail address: Khurshid@cuiatd.edu.pk (K. Ayub).

https://doi.org/10.1016/j.ijhydene.2023.03.018

Introduction

World energy consumption is increasing exponentially with increase in world population. The natural energy resources are also rapidly depleting with time. Moreover, these fossil fuels cause emission of several harmful gases, therefore, the world is facing considerable power and environmental problems [1]. The limited and nonrenewable fossil fuel energy resources and their impact on environment requires a shift to renewable energy resources [2]. Considering the depletion and environmental impacts of fossil energy resources, hydrogen can be considered as an ideal energy carrier which can be easily generated in bulk from renewable resources. Hydrogen energy has numerous advantages, including facile production, high energy density and easy conversion to other forms of energy. Moreover, the only byproduct of hydrogen combustion is water. Furthermore, Hydrogen has higher utilization efficiency, high environmental compatibility and is also the most suitable fuel for vehicle application [3]. Therefore, hydrogen can be considered as a best alternative to replace fossil fuels.

In hydrogen dissociation, the H_2 molecule splits into active hydrogen atoms which are then incorporated into the support material or catalyst, making it possible to store large amounts of hydrogen at low temperatures and pressure [4,5]. The rate of hydrogen dissociation reaction of a metal/hydrogen system is a function of temperature and pressure. Moreover, the metal surface must possess the ability to split the H_2 molecule and allow easy diffusion of active hydrogen atoms, thereby enabling hydrogen storage. The dissociation ability of different metals is different depending on their intrinsic properties [6]. Moreover, in hydrogenation reactions, hydrogen dissociation is considered among the rate limiting steps. Therefore, the nature of active sites for H_2 dissociation over metal catalysts is the subject of interest for various studies [7]. Moreover, catalytic adsorption and dissociation of molecular hydrogen is of great interest in hydrogenation and dehydrogenation reactions at commercial level. In such reactions, molecular hydrogen is first adsorbed on the catalyst surface and then, dissociated into active hydrogen atoms. Therefore, it is necessary to understand the elementary steps involved in hydrogen dissociation and in the development of highly efficient catalysts [8]. One of the major challenges encountered in the development of the hydrogen economy is the storage capability of hydrogen efficiently and safely [9].

Previously many noble metals (Ru, Au, Pd, Pt, and Rh) have been reported to catalyze the hydrogen dissociation process efficiently [10–14]. Previously the most common type of catalysts studied for the dissociation of H_2 molecules include different precious metals based catalysts (e.g. Pt, Pd, Rh & Ru) [15,16], metal oxides (e.g. Cr_2O_3, Nb_2O_5, TiO_2 & Fe_3O_4) [16], and non-metals compounds (e.g. carbon) [17,18]. However, the main problems with these noble metal catalysts include high operation temperature and high cost which render these catalysts, hence not economically feasible [19]. In this regard, first row transition series metals such as Sc, Fe, Mn, Ni, Co, and Cu *etc.*, can be considered as best alternatives due to low cost and high relative abundance [20,21]. For practical applications and large-scale production, it is necessary to replace noble expensive metal catalysts with low cost and environment friendly catalysts.

Moreover, to further reduce the cost while maintaining the performance of catalysts, the best approach is to employ single atom catalysis (SAC). Currently, SAC has been considered as best choice, where single metal atom is anchored on a support to accomplish the desired catalytic activity [22–24]. The catalytic performance of SACs is now taking hold, but the understanding of the catalytic process of such catalysts is still in its infancy. The noble metal Pd decorated graphene surface has been studied for hydrogen dissociation reaction by Yan et al. and they observed a moderate energy barrier of 0.84 eV [25]. Therefore, the catalysis of single metal atom anchored on some support is of great research interest [24]. Researchers are still attempting to design SACs, which could offer economical, robust, and highly selective electrocatalysis with minimal barrier for hydrogen dissociation process.

In this regard, carbon-based materials such as organic frameworks [26,27], graphene [28,29], graphyne [30], graphitic carbon nitride (g-C_3N_4) [31], and other nanostructured surfaces have received much attention as support materials (for catalyst) due to their higher surface area and promising storage capacities at low temperature [32–34]. Recently, low cost and abundantly present transition metals (Fe, Co, & Ni) doped C_2N surface has been investigated for H_2 dissociation process [35].

Similarly, various 2D materials have been studied and reported in literature for hydrogen dissociation such as carbon-based surfaces [36–38], carbon nanotubes [39] and quantum dots [40,41]. The dissociation barrier for the hydrogen molecule were reported about 3.51 eV and 3.70 eV on the pristine and 1, 3-cyclohexadiene (CHD) functionalized CNT, respectively [8]. Moreover, Wan et al. studied the adsorption and dissociation of Hydrogen on Au supported TiO_2 catalysts and observed lower H_2 dissociation barrier of 0.10 eV over stoichiometric Au/TiO2(101) surface [5]. Furthermore, Pozzo et al. theoretically studied H_2 dissociation on transition metals (TM = Ti, V, Ni, Cu, Ag etc.)-doped Mg surfaces and their results revealed Ni-doped Mg being the best choice [9]. Furthermore, isolated individual Pd atoms were also investigated both experimentally and theoretically, and results revealed that Pd atoms can promote the hydrogen dissociation reaction efficiently [42]. Investigation of low cost and highly abundant metals (e.g., Mg, Sc, Mn, Ni etc.) for hydrogen dissociation process is the subject of interest for researchers due to their low cost and higher capacities for hydrogen storage [8]. Nonetheless, scientists are still trying to find an appropriate electrocatalyst with can efficiently catalyzed hydrogen dissociation reaction.

Current study explores particularly the highly stable and smaller variant of fullerene (TMs doped C24) for hydrogen dissociation reaction. Recently, fullerenes, an allotropic form of carbon have gained significant interests owing to their unique characteristics. In fullerenes, carbon atoms (sp2 hybridized) are linked to form the hollow sphere of various sizes i.e., C20, C24, C30, C60 etc. Small sized fullerene nanocages such as C20 and C24, exhibit remarkable properties due to highly pyramidalized C-atoms and large curvature in their structures. Different types of fullerenes nanocages have been recently researched for their hydrogen energy applications. Although small fullerenes (C20–C30) have stability issue

[43,44], but literature reveal that C24 nanocage exhibits stable geometry which is maintained even after chemical modifications [45,46]. An extensive study by Jensen et al. on small sized fullerenes revealed that C24 favours D_6 symmetry over O_h symmetry [47–49]. Their catalytic properties can be enhanced by chemical modifications such as metal decoration and doping.

With the motivation of designing efficient SACs for hydrogen dissociation, we have selected the most stable symmetry (*D6*) of C24 nanocage as a support material [23]. C24 nanocage is functionalized with first row TMs (Sc, Ti, V, Cr, Mn, Fe, Co, Ni, Cu & Zn) to improve the H_2 adsorption characteristics. In this study, we have systemically probed first-row TMs (Sc—Zn) as SACs doped on C24 nanocage through density functional theory (DFT) calculations and demonstrated their stability, and catalytic activity for H_2 dissociation process.

Methodology

DFT calculations for gas phase geometry optimization have been performed using B3LYP/6-31G(d,p) level of theory using Gaussian 09 software [50]. B3LYP is a hybrid DFT functional which is well known for computation of electronic properties, thermodynamic stabilities, and reaction barriers of fullerenes [51–53]. Vibrational frequencies are also computed at the same level of theory to analyze stationary points on potential energy surface (PES). GaussView 5.0 package and Chemcraft were used to visualize the optimized geometries [54]. The optimized geometries are confirmed through frequency analysis. Reactants and products of the studied complexes are considered as minima when no negative or imaginary frequency is observed. Whereas transition states are confirmed when one imaginary frequency is present. All the transition states are further evaluated through their associated eigenvectors which correspond to the motion along the reaction coordinates [55]. The solvation effect on dissociation mechanism is also evaluated through polarizable continuum model (PCM) in aqueous media at the same level of theory [56].

To obtain the stable TM@C24 complex, transition metals are adsorbed at different positions; b6,5 and b5,5 interfaces. The first-row transition metals (TMs) supported on C24 cage has been used to catalyze the hydrogen dissociation reaction. C24 fullerene is doped with first-row transition metals exohedrally. TMs show multiple spin states; hence, four lowest possible spin states (up to octet and septet) are considered to get the lowest or the most thermodynamically stable spin state. The adsorption energies and hydrogen dissociation reactions of TM@C24 complexes are also performed on the most stable spin states.

Adsorption energies (E_{ads}) of TMs over C24 nanocages are calculated for the stable spin states through the following expression:

$$\Delta E_{ads} = E_{TM@C24} - (E_{C24} + E_{TM}) \quad (1)$$

Here, $E_{T.M@C24}$, E_{C24} and $E_{T.M}$ are the energies of $TM@C_{24}$ complexes, bare C_{24} surface and TMs with the most stable spin state, respectively.

To further estimate the binding strength of H_2 on $TM@C_{24}$ nanocages, adsorption energy ΔE_{ads} (H_2) by eq (2) is also calculated. In eq (2), $E_{H2TM@C24}$ is the total energy of the H_2 adsorbed TM@C24 nanocage complexes, E_{H2} is the energy of isolated H_2 molecule, and $E_{TM@C24}$ represents the energy of optimized TM@C24 nanocage complexes.

$$\Delta E_{ads}\,(H_2) = E_{H2TM@C24} - (E_{TM@C24} + E_{H2}) \quad (2)$$

The activation and self-dissociation of H_2 molecule is further elaborated through NBO and EDD analysis. NBO analyses is performed at B3LYP/6-31G(d,p) level of theory, which indicates the nature of bonding in view of orbital interactions and charge transfer. Furthermore, EDD analysis is also carried out for the stable TM@C24 nanocage complexes. The EDD is evaluated by subtracting the electronic density of H_2 and TM@C24 nanocage from the electronic density of the H_2TM@C24 nanocage complexes. Moreover, noncovalent interactions (NCI) analysis is performed to confirm the existence of shared shell interactions between TMs and C-atoms of nanocage.

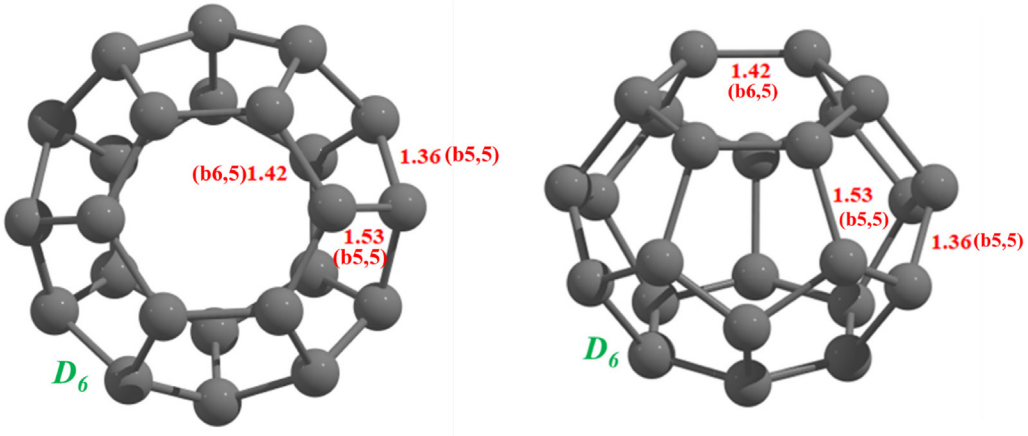

(a) (b)

Fig. 1 – The optimized geometry of C24 nanocage with D_6 symmetry, (a) top view and (b) side view.

Results and discussion

Geometry optimization and adsorption energy

First row transition metals are selected as dopant for C24 replace noble metal catalyst to investigate H_2 dissociation process. The most stable symmetry for C24 fullerene is D_6. Literature reveals the energetic stability of D_6.symmetry of C24 fullerene over O_h symmetry [47,48]. Thus, C24 fullerenes with D_6 symmetry is chosen and the computed topology of C24 nanocage is given in Fig. 1 (both side and top views). C24 fullerene consists of twelve pentagonal faces and has two hexagons. Therefore, the relaxed geometry of C24 nanocage consists of two different types of C–C bonds. The one bond is common at interface of hexagon and pentagon rings, which is termed as b6,5. The second type of bond is termed as b5,5 which is shared between two pentagons. The bond length of 1.42 Å is observed for b6,5, whereas the two types of bond lengths (1.53 Å and 1.36 Å) are observed in case of b5,5 (see

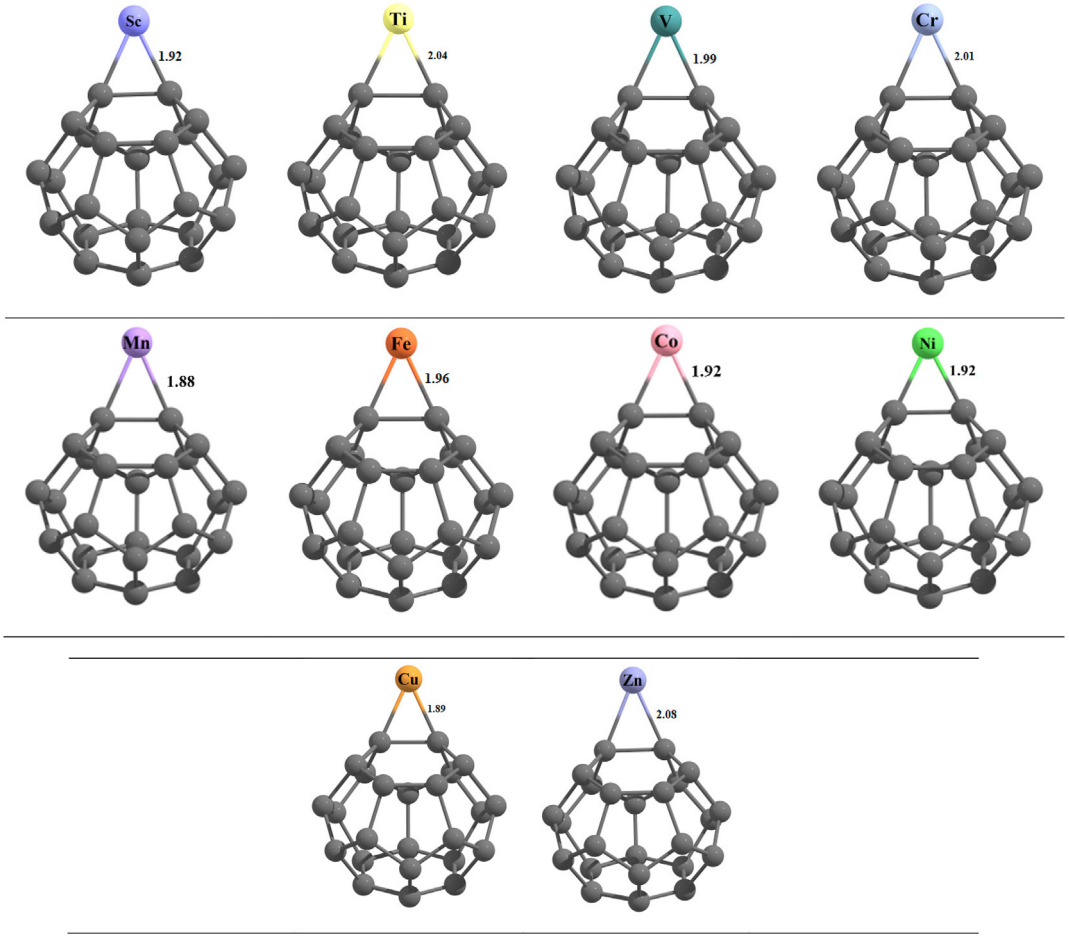

Fig. 2 – Optimized geometries of stable TMs@C24 nanocage complexes at B3LYP/6-31G(d,p) level of theory.

Table 1 – Summary of energies for the adsorption of TM over C24 nanocage, H_2 adsorption over TM@C24, and energy barriers for hydrogen dissociation reaction in gas phase as well as in aqueous media.

Complexes	Gas phase	Solvent	Complexes	Gas phase		Solvent (H_2O)	
	ΔE_{ads} (eV)	$\Delta E'_{ads}$ (eV)		ΔE_{ads} (eV)	ΔE_a (eV)	$\Delta E'_{ads}$ (eV)	$\Delta E'_a$ (eV)
Sc@C24	−3.99	−6.01	H_2Sc@C24	−0.04	0.76	−0.43	0.49
Ti@C24	−3.42	−5.86	H_2Ti@C24	−0.22	0.66	−0.20	0.60
V@C24	−2.10	−3.92	H_2V@C24	−0.53	1.00	−0.16	0.47
Cr@C24	−2.78	−3.84	H_2Cr@C24	−0.15	1.08	−0.14	0.43
Mn@C24	−6.22	−6.11	H_2Mn@C24	−0.22	0.04	−0.19	0.30
Fe@C24	−3.99	−3.23	H_2Fe@C24	−0.45	0.30	−0.13	0.77
Co@C24	−3.42	−3.56	H_2Co@C24	−0.29	0.36	−0.29	0.63
Ni@C24	−2.10	−5.80	H_2Ni@C24	−0.88	0.65	−0.52	0.74
Cu@C24	−3.24	−3.83	H_2Cu@C24	−0.56	0.48	−0.29	0.74
Zn@C24	−0.26	−1.58	H_2Zn@C24	−0.05	0.84	−0.10	1.50

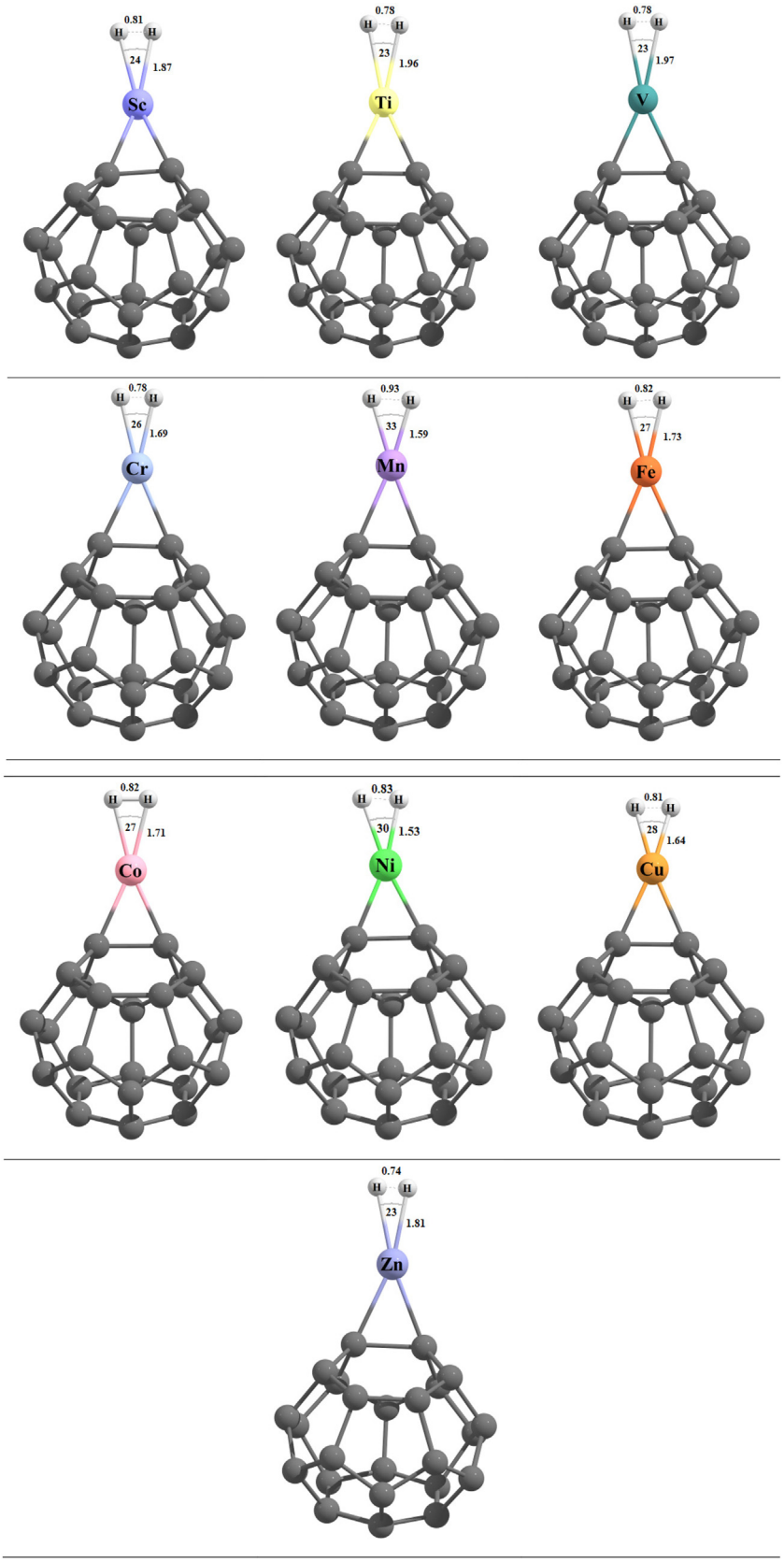

Fig. 3 – Optimized geometries of hydrogen doped TMs@C24 nanocage complexes at B3LYP/6-31G(d,p) level of theory.

Fig. 1), which are in good agreement with previously reported results [3].

Initially, TM is placed at different positions (b6,5 and b5,5 interfaces) on the surface of C24 fullerene (hexahedral) to find the most stable TM@C24 nanocage complex. In all studied complexes, the most stable complex is seen on b5,6 position. Furthermore, first four possible spin state of each TM@C24 are evaluated to explore thermodynamically stable complex. The most stable spin state observed for Sc@C24, V@C24, Mn@C24, and Co@C24 is quartet, whereas for Cu@C24 complex, doublet is the most stable spin state. Similarly, for Ti@C24, Cr@C24, and Fe@C24, the most stable spin state is quintet and Ni@C24 and Zn@C24 complexes are more stable in singlet spin state. The relative energies of various spin states of first-row TM@C24 nanocage complexes are presented in Table S1 (Supporting info) whereas the most stable spin state geometries and their adsorption energies over C24 nanocage complex are given in Fig. 2 and Table 1. It is observed from Fig. 2 that interaction distances between transition metal and C24 nanocage are in the range of 1.88 Å to 2.08 Å, which primarily reveal chemisorption. The lowest interaction distance is observed in case of Mn@C24 complex (1.88 Å) for each Mn–C bond. The lowest bond length in Mn@C24 complex is also justified from the highest adsorption energy (ΔE_{ads}) value. Whereas the highest interaction distance among all studied complexes is 2.08 Å, observed for Zn@C24 complex. The observed interaction distances between the C24 nanocage and TM for all studied complexes are almost comparable with their TM—C bond lengths reported in literature [57].

The adsorption energies of most of the TM complexes in various spin states are related to the number of unpaired electrons. The negative sign of adsorption energies of TM@C24 complexes indicates the adsorption of TM on C24 nanocage is an exothermic process. The adsorption energies of TM@C24 complexes range from −0.26 eV to −6.22 eV. Thus, all the studied complexes are thermodynamically stable. The highest adsorption energy (ΔE_{ads}) is observed for the Mn@C24 nanocage complex (−6.22 eV) owing to the higher thermodynamic stability of this catalyst. The least adsorption energy is calculated for the Zn@C24 catalyst (−0.26 eV). Moreover, adsorption energy ($\Delta E'_{ads}$) values are computed using CPCM model to evaluate the solvent effect. In this case, the adsorption energy values are observed in the range of −1.58 eV (Zn@C24) to −6.11 eV (Mn@C24). The trend of adsorption energy values observed with solvent are consistent with the gas phase values. The results of adsorption energies are also validated through the interaction distances of TM@C24 complexes.

H_2 adsorption over TM@C24 catalysts

The H–H bond distance (d_{H-H}) for the hydrogen adsorbed on non-noble transition metal anchored TM@C24 nanocages lie in the range of 0.74 and 0.93 Å (see Fig. 3). Adsorption energy for the adsorption of H_2 molecules over TM@C24 complexes is also calculated and presented in Table 1. In some cases, the H–H bond distance is slightly larger than isolated H_2 molecule (H–H bond length; 0.74 Å), which might be attributed to strong TM—H bond interactions, ultimately weakening the H–H bond. All the studied complexes are favorable energetically for hydrogen adsorption and calculated adsorption energies are in the range of −0.04 to −0.88 eV. Moreover, the Ni@C24 (−0.88 eV) and Cu@C24 (−0.56 eV) catalysts have shown relatively stronger H_2 adsorption (see Table 1 for details). Higher negative values present strong binding of H_2 molecule to the TM@C24 nanocage. Overall, the Cr@C24 catalyst has the least adsorption of hydrogen molecules among all ten studied TM@C24 catalysts, whereas the strongest adsorption of hydrogen molecules is observed over Sc@C24 and Mn@C24 catalysts.

The adsorption of hydrogen molecule over studied TM@C24 catalysts is also evaluated using CPCM model to

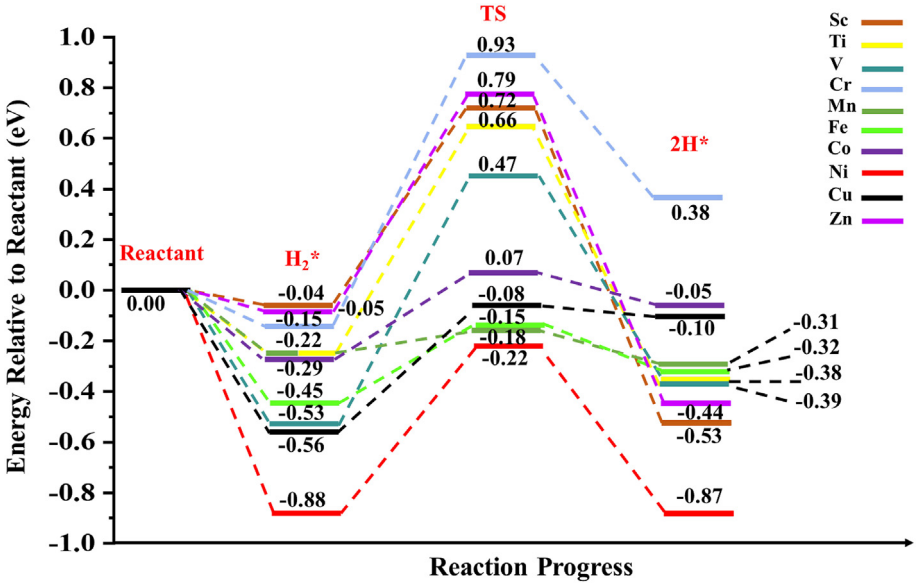

Fig. 4 – Reaction pathways for hydrogen dissociation reaction on TM@C24 (TM = Sc–Zn) catalysts; the energies of intermediate (H_2*), transition state (TS) and products (2H*) are relative to reactants and are expressed in units of eV.

check the solvent effect. In the presence of aqueous media (solvent), the adsorption energy ($\Delta E'_{ads}$) values are observed in the range of −0.10 eV to −0.52 eV, which reveals that all the studied complexes are energetically favorable for hydrogen adsorption process. In this case, the highest adsorption energy value is observed for $H_2Ni@C24$ complex (−0.52 eV) followed by $H_2Sc@C24$ (−0.43 eV), $H_2Cu@C24$ and $H_2Co@C24$ (−0.29 eV each) complexes owing to higher thermodynamic stability of these catalysts. Again, the trend is almost consistent with the gas phase calculations but with the slight increase in the overall energy values.

Metal hydrogen (TM—H) bond distances vary in different systems, and range from 1.53 Å to 1.97 Å, where the Ni—H (1.53 Å) and Mn—H (1.59 Å) being the shortest among all (see Fig. 3). Overall, adsorption of H_2 molecule at the TM@C24 nanocages (two H* for TM@C24), increases the bond length of H—H bond slightly. These results reveal the activation of H_2 molecule at single metal atom site.

Dissociation of hydrogen molecule over TM@C24 nanocages

To explore the best performance of the studied TM@C24 catalyst for the catalytic cleavage of hydrogen molecule, homolytic dissociation reaction of the adsorbed hydrogen molecule is evaluated. The results further demonstrate that the 2H* state is energetically more favorable for all the studied TM@C24 catalysts because of exothermic process (negative energy) except Cr@C24 nanocage (see Fig. 4). The dissociation of hydrogen molecule can be achieved in two steps: the step I is the adsorption of hydrogen molecule resulting in an intermediate formation and step II involves the homolytic cleavage (in most cases) of hydrogen molecule and binding of two hydrogen atoms on the same metal atom.

Among studied H2M@C24 complexes for homolytic dissociation, the lowest energy barrier for hydrogen dissociation is calculated for Mn@C24 catalyst (0.04 eV), whereas the highest barrier is seen for Cr@C24 catalyst (1.08 eV). Moreover, the dissociation barrier for H_2 molecule over a Fe@C24 (0.30 eV) and Co@C24 (0.36 eV) catalysts are almost comparable with a difference of 0.06 eV. The observed dissociation barrier for Cu@C24 catalyst is 0.48 eV, which is even smaller than the reported Cu@Mg surface (0.56 eV) [9]. For the rest of the studied complexes, the dissociation barriers are 0.76, 0.66, 1.00, 0.65 and 0.84 eV for Sc@C24, Ti@C24, V@C24, Ni@C24 and Zn@C24, respectively. The summary of some of the important bond lengths (Å) and bond angles (deg) at intermediate, transition state and product of $H_2TM@C24$ nanocage complexes are reported in Table S2 (Supporting info). Table S2 (supporting information) reveals that the hydrogen dissociation process in most of the studied TM@C24 complexes follows early transition state trend based on H—H bond distance. In case of early transition state, the geometry is closer to the geometry of the reactant molecule, taking small activation energy, and vice versa. The shorter H—H bond distance at transition state

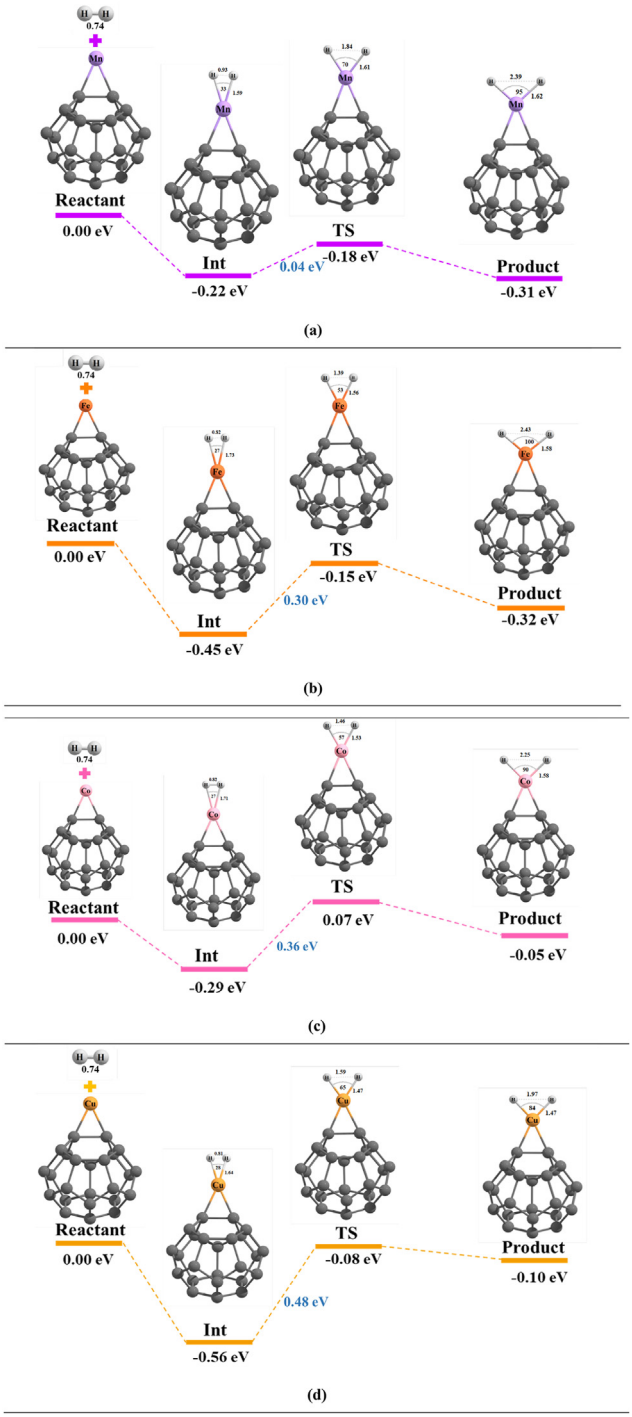

Fig. 5 – The schematic diagrams of reactant, intermediate (Int), transition state (TS), and product are demonstrated by side views (H, white; C, grey; Mn, purple; Fe, orange; Co, pink; Cu, brown). (a) Mn@C24, (b) Fe@C24, (c) Cr@C24 and (d) Cu@C24. (For interpretation of the references to color in this figure legend, the reader is referred to the Web version of this article.)

Table 2 – Bond order calculation results for studied TM@C24 complexes at TS.

Complexes	B.O. (TM—H)	B.O. (H—H)	Complexes	B.O. (TM—H)	B.O. (H—H)
$H_2Sc@C24$	0.53	0.17	$H_2Fe@C24$	0.49	0.23
$H_2Ti@C24$	0.45	0.37	$H_2Co@C24$	0.52	0.20
$H_2V@C24$	0.44	0.27	$H_2Ni@C24$	0.54	0.17
$H_2Cr@C24$	0.48	0.33	$H_2Cu@C24$	0.74	0.06
$H_2Mn@C24$	0.75	0.05	$H_2Zn@C24$	0.53	0.27

reveals an early transition state. Late transition state trend is observed in case of Mn@C24 and Cu@C24 complexes as the geometric parameters resemble more like product states. While in all remaining complexes the early transition state trend is observed.

Herein, Mn@C24 catalyst is selected as a representative model to investigate the hydrogen dissociation process. In addition, all those M@C24 complexes (Mn@C24, Fe@C24, Co@C24 and Cu@C24), which show better catalytic efficiency, are presented in Fig. 5. Whereas energy diagrams of the rest of studied TM@C24 complexes are given in supporting information (Figs. S1–S6). The adsorption of Mn atom on C24 occurred at common interface b6,5 of C24 nanocage. The observed C–Mn bond length is 2.03 Å between Mn atom and C atoms of C24 nanocage directly attached to Mn, which is in agreement with previously reported results [58]. To study dissociation of H_2 over Mn-doped C24 nanocage, initially H_2 is adsorbed over Mn@C24 nanocage. The adsorption energy of −0.51 eV is observed, which is better than all other studied systems except Sc@C24 complex (−0.53 eV). The observed interaction distance between Mn and H-atoms of H_2 molecule are 1.59 Å each. The H–H bond length in H_2–Mn@C24 complex is 0.93 Å, which is slightly increased as compared to isolated H_2 molecule i.e., 0.74 Å (see Fig. 5). This elongation in bond length of H_2 molecule upon adsorption reveals the activation of the H_2 molecule over Mn@C24 nanocage complex.

Transition state reveals that H_2 dissociation is proceeded through homolytic cleavage of hydrogen molecule. Homolytic cleavage or oxidative addition of H_2 molecule is more common in electron rich metal centers. This type of oxidative addition proceeds through the donation of electrons from TM to σ* of H–H bond. The H–H bond length is increased from 0.93 Å to 1.84 Å, whereas bond angle is increased from 33° to 70°, respectively. The H–H bond distance (D_{H-H}) is a crucial structural parameter in the dissociation process, that may demonstrate the stability of transition state. Our results agree with the previously reported theoretical reports for H–H bond distance in the transition state and even more pronounced compared to previously reported literature [59–62].

The hydrogen dissociation over Mn@C24 complex has late transition state, meaning that the geometry of transition state is more like the product molecule. The H–H bond length at transition state is 1.84 Å closer to the H–H bon distance of dissociated hydrogen atoms (2.39 Å) as compared to reactant (0.93 Å). Therefore, this late transition state contributes to lowering of activation barrier (0.04 eV) by stabilizing the H_2 molecule over Mn@C24 catalyst. According to bond order calculations, at **TS**, Mn@C24 catalyst shows almost covalent linkage with both hydrogen atoms (Mn–H) with bond order value of 0.75 (single bond). Whereas the bond order value for H–H bond is 0.05, which shows that at **TS** the complex has similarity with the product side (2H*+Mn@C24). At **TS**, the Mn@C20 catalyst is strongly interacted with hydrogen atoms which marks the dissociation of H–H bond quite easily. Moreover, in all those cases where early TS observed the bond order for M—H is in the range of 0.44–0.54 owing to partial single bond (see Table 2).

This barrier is the lowest among all 1st row TMs doped C24 nanocage complexes. This shows that Mn doped C24 nanocage showed best catalytic activity compared to rest of studied 1st row TM complexes. The activation barrier is even smaller than noble metal doped CeO_2, where the activation barrier of 0.25 eV was reported in the literature [58,63]. On product side, hydrogen dissociation proceeds with further increase in bond length and bond angle to 2.39 Å and 95°, respectively. No deformation is observed in C24 fullerene in case of Mn@C24 nanocage after H_2 adsorption, which indicates the stability of C24 nanocage for single atom catalysis. Furthermore, the enthalpy of reactant and product of $H_2Mn@C24$ complexes reveals that product is more stable than reactants. The negative enthalpy values in case of intermediate and product reveal the feasibility of H_2 dissociation reaction over Mn@C24 nanocage complex.

Table 1 reveals that the barriers for dissociation of hydrogen molecules on the studied ten transition metal (TM@C24) catalysts are in the wider range of 0.04 eV–1.08 eV. Notably, the lowest energy barrier is observed for Mn@C24 catalyst, which is only 0.04 eV, much smaller than the other nine candidates. Moreover, it is noticed that metal–H interaction is very important for a homolytic cleavage of molecular hydrogen. The Mn@C24 complex based on SAC gives best hydrogen dissociation activity as compared to other studied TM@C24 complexes. Therefore, Mn@C24 complex can be considered as promising single atom catalyst to catalyze the hydrogen dissociation process efficiently.

Furthermore, the hydrogen dissociation reaction is also evaluated using CPCM model to check the solvent effect upon reaction mechanism. The energy barriers ($\Delta E'_a$) for HDR in water are reported in Table 1, which reveal that the dissociation barriers for hydrogen dissociation are in the range of 0.30 eV–1.50 eV. The lowest energy barrier in this case is calculated for Mn@C24 catalyst (0.30 eV) is consistent with gas phase results followed by Cr@C24 catalyst (0.43 eV). For V@C24, this barrier is 0.47 eV followed by Sc@C24 (0.49 eV) and Ti@C24 (0.60 eV) catalysts. In case of early transition metal from Sc to Cr, a decrease in dissociation barriers is observed in

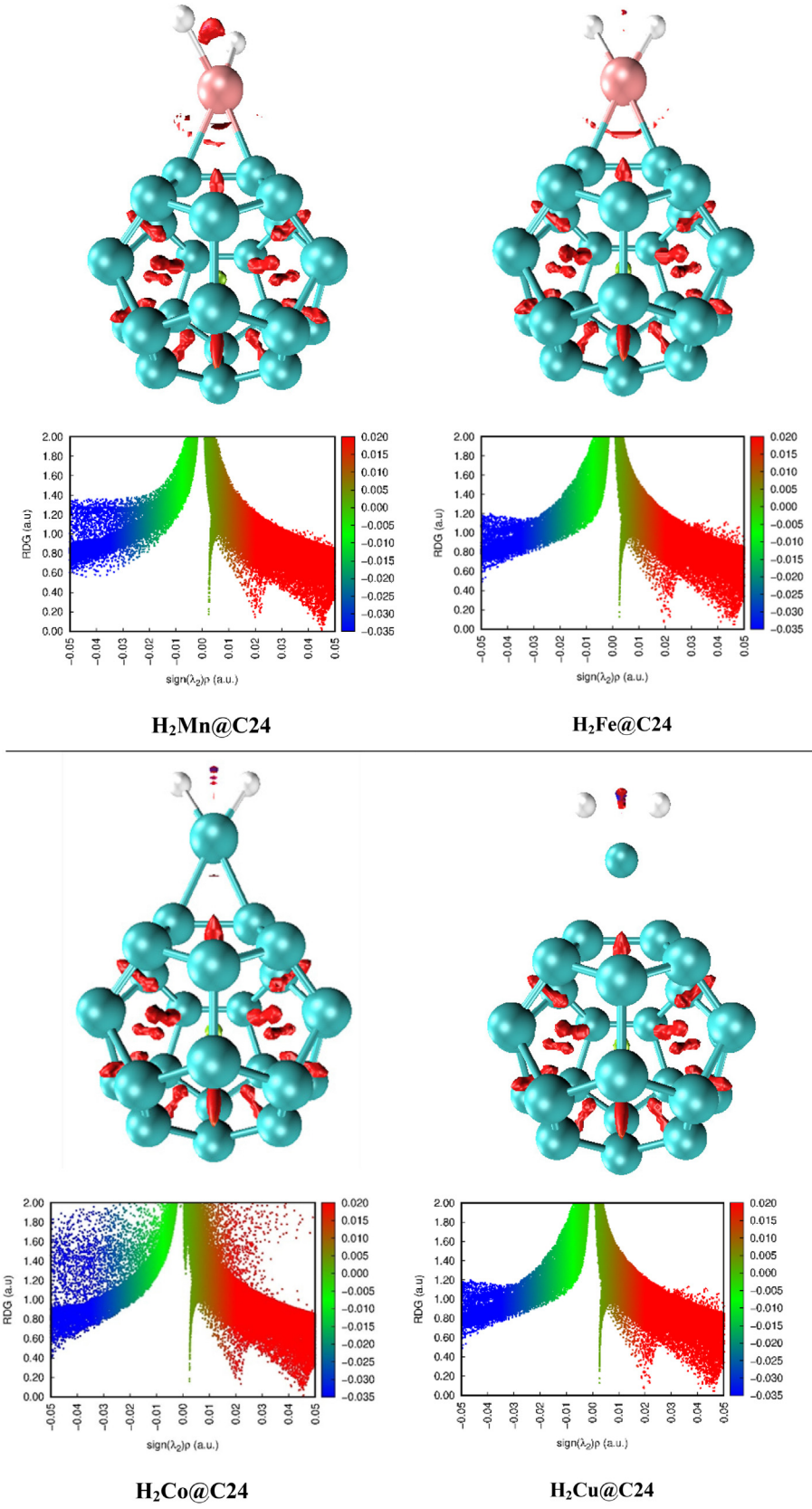

Fig. 6 – RDG isosurfaces and 2D RDG spectra of representative TM@C24 complexes.

Table 3 – NBO analysis results of considered studied stable hydrogen adsorbed TMs@C24 complexes.

Complexes	H1 (e^-)	H2 (e^-)	TM (e^-)	C1 (e^-)	C2 (e^-)
$H_2Sc@C24$	−0.217	−0.260	1.369	−0.371	−0.289
$H_2Ti@C24$	−0.200	−0.200	1.125	−0.407	−0.407
$H_2V@C24$	−0.215	−0.197	1.265	−0.379	−0.382
$H_2Cr@C24$	−0.192	−0.199	0.932	−0.348	−0.355
$H_2Mn@C24$	−0.210	−0.260	1.080	−0.350	−0.380
$H_2Fe@C24$	−0.090	−0.090	0.514	−0.270	−0.270
$H_2Co@C24$	−0.153	−0.153	0.827	−0.368	−0.368
$H_2Ni@C24$	−0.143	−0.113	0.547	−0.325	−0.273
$H_2Cu@C24$	0.002	0.002	0.171	−0.200	−0.200
$H_2Zn@C24$	−0.075	−0.074	0.909	−0.372	−0.368

aqueous media (see Table 1). Whereas for late transition metals (Mn to Zn), increase in activation barriers is observed in the presence of solvent. Usually, in polar solvents the activation barriers are higher than gas phase [64]. These findings reveal that H_2 dissociation mechanism in the solvent stays the same as in the gas phase however, the dissociation barriers are slightly different than those of gas phase.

Reduced density gradient (RDG) analysis

RDG analysis is also performed, which is usually used to detect the noncovalent interactions in real space based on electron density. Here, we carried out the RDG analysis to confirm the presence or absence of close shell interactions (non-covalent interactions) in $H_2M@C24$ complexes. For close shell interactions, the electron density (ρ) should be > -0.02 a.u [65]. RDG analysis is performed using Multiwfn 3.7 program [66], and grid points are obtained as function of two variables; sign(λ_2)ρ as function 1 (x-axis) and RDG as function 2 (y-axis). For 3D color isosurfaces, VMD program is employed [67]. The RDG isosurfaces and 2D plots for the representative complexes ($H_2Mn@C24$, $H_2Fe@C24$, $H_2Co@C24$ and $H_2Cu@C24$ complexes) are given in Fig. 6, while the rest are given in supporting information (Fig. S7). NCI analysis reveals the absence of non-covalent interactions between H_2 and M@C24 complexes. Similarly, in 2D NCI plots, spikes about non-covalent interactions (van der Waals or H-bonding) are not observed. These plots shows that interactions between H—M and M—C in $H_2M@C24$ complexes are covalent in interactions which is perfect for catalysis reactions. The electronegativities of transition metals are almost comparable with that of hydrogen, thus the resulting M–H bonds are predominantly covalent in nature in case of homolytic cleavage. The obtained results are also consistent with the already reported metal doped phosphides and nitrides surfaces for hydrogen dissociation study, where M—H bond was covalent in nature [68]. The covalent or strong interaction of analyte over catalyst will promote the dissociation of H_2 molecule into active H* atoms. Moreover, the shared shell interactions (steric strain) are also confirmed through red cylindrical projections as presented in 3D isosurface (Fig. 6).

Electron density differences (EDD) and natural bond orbital (NBO) analysis

The activation and self-dissociation of H_2 molecule is further elaborated through NBO and EDD analysis. To exactly estimate the amount of charge transfer occurred from the 3d orbitals of transition metals upon adsorption of H_2 molecule, we have performed the NBO analysis of our studied TM@C24 complexes (see Table 3). In TM@C24 complexes, the positive NBO charge is observed on TMs in all considered complexes, whereas negative NBO charge values are observed on carbon atoms directly attached with the TM atoms. The calculated NBO charges for all considered complexes are reported in Table 3. NBO analysis reveals that the charge is being transferred from TMs to C24 and H_2 atoms owing to electropositive nature of metals. The positive charge on TMs is an obvious reason of charge transfer from metal atoms to the C24 support in all studied complexes. The highest charge transfer is observed for Sc metal (+1.37 e^-), whereas the least charge transfer is observed for Cu metal (+0.17 e^-).

Herein, we only discuss the charge transfer of representative model in detail i.e., Mn@C24 fullerene complex. In case of $H_2Mn@C24$ nanocage, a charge of +1.08 e^- is examined on Mn, while charges of −0.25 e^- and −0.38 e^- is noticed on carbons of C24 which are directly attached to Mn metal atom i.e., C1 and C2, respectively. At transition state, where H_2 self-dissociation happened over Mn@C24 complex, charge of −0.21 e^- and −0.26 e^- is seen for H1 and H2 atoms, respectively, whereas charges on metal remained +1.08 e^-. This increase in positive charge on metal indicates the charge transfer from metal to H-atoms. Overall, this charge transfer shows strong binding interactions of TM atom with H_2 molecules which causes its dissociations. This charge transfer from TM atom to hydrogen atoms, is mainly responsible for the elongation of the H–H bond, thus facilitating the process of H_2 dissociation over TM@C24 complexes. NBO analysis reveals the transfer of charge from TM to H_2 molecule, thus filling up antibonding orbital of hydrogen and hence results in the dissociation of H–H bond.

Electron density differences (EDD) is performed to validate the results of NBO charge transfer from TM@C24 complexes to H_2. The obtained EDD isosurfaces for studied $H_2TM@C24$ complexes are given in Fig. 7. The EDD isosurfaces exhibit cyan blue and violet patches, therefore, reveal the charge transfer upon adsorption of H_2 molecule. Cyan blue isosurfaces show the depletion of electron density, whereas violet isosurfaces depict accumulation of electronic density. EDD analysis clearly reveals that, in all studied complexes, the charge is transferred from TMs to H_2 atoms (see Fig. 7). In all complexes, the cyan blue patches are present over metal atoms presenting the depletion of electronic density, whereas violet isosurfaces are observed over H atoms and C atoms. The

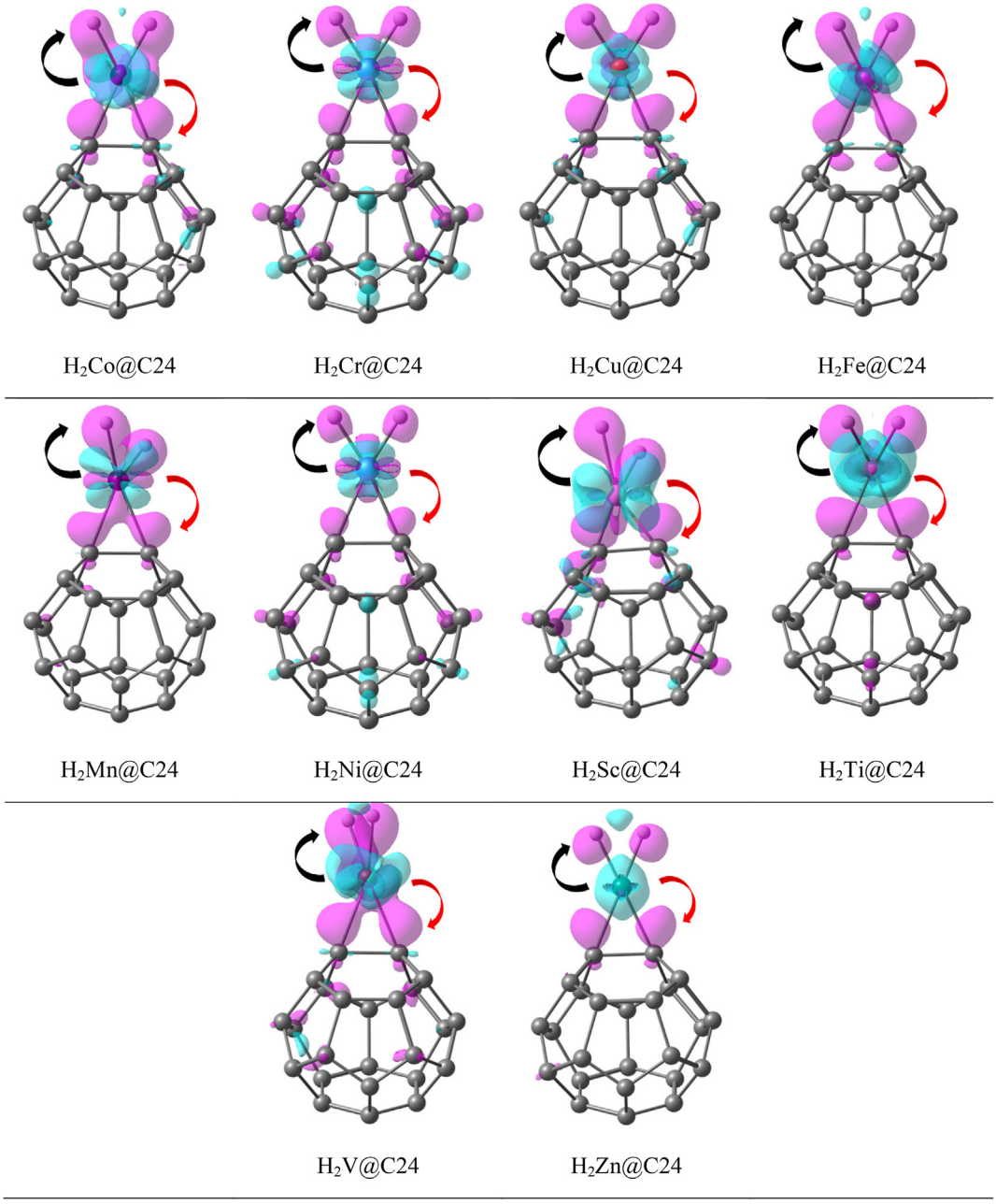

Fig. 7 – EDD isosurfaces of studied TMs@C24 nanocage complexes, violet isosurfaces present the accumulation of electron density, whereas cyan blue isosurfaces show the depletion of electron density. (For interpretation of the references to color in this figure legend, the reader is referred to the Web version of this article.)

outcomes of EDD analysis show strong agreement with the results of NBO charge analysis.

Conclusions

In this work, the adsorption and dissociation of the H_2 molecule has been investigated on TM@C24 complexes through DFT method. Adsorption of TM on C24 nanocage is exothermic in TM@C24 complexes. The highest adsorption energy (−6.22 eV) is calculated for Mn@C24 catalyst. NCI analysis is performed to confirm the shared shell or covalent interactions between hydrogen atoms and TM@C24 complexes. The RDG results reveal that covalent interactions promote the dissociation of H_2 molecule over TM@C24 complexes into active H* atoms. Furthermore, H_2 adsorption on C24 nanocage, and dissociation barriers are also compared systematically for first the row TMs doped C24 complexes. The results declare that the 2H* state is energetically more favorable for studied TM@C24 catalysts due negative energy (exothermic process) except Cr@C24 nanocage. It is further observed that the H_2 dissociation barrier on Mn@C24 complex (0.04 eV) is the lowest among all studied complexes. The activation and dissociation process of H_2 molecule is further

elaborated through NBO and EDD analysis. Solvent effect on dissociation mechanism is also evaluated, which indicates that the H_2 dissociation mechanism in the solvent stays the same, however the dissociation barriers are slightly different than those of gas phase. This study reveals that Mn@C24 nanocage can be used as an efficient electrocatalyst for H_2 dissociation reaction. Moreover, this research provides new avenue to experimentalists to design efficient and high-performance SAC for H_2 dissociation process.

Declaration of competing interest

The authors declare that they have no known competing financial interests or personal relationships that could have appeared to influence the work reported in this paper.

Acknowledgment

This study was supported by Higher Education Commission of Pakistan under HEC indigenous fellowship to Sehrish Sarfaraz (PIN) 520-141149-2PS6-178 (50093367) and COMSATS University Islamabad, Abbottabad Campus for financial support.

Appendix A. Supplementary data

Supplementary data to this article can be found online at https://doi.org/10.1016/j.ijhydene.2023.03.018.

REFERENCES

[1] Mahdizadeh SJ, Goharshadi E. Hydrogen storage on silicon, carbon, and silicon carbide nanotubes: a combined quantum mechanics and grand canonical Monte Carlo simulation study. Int J Hydrogen Energy 2014;39(4):1719–31.
[2] Hirose K. Handbook of hydrogen storage: new materials for future energy storage. John Wiley & Sons; 2010.
[3] Sathe RY, et al. Hydrogen storage capacity of low-lying isomer of C24 functionalized with Ti. Int J Hydrogen Energy 2020;45(16):9936–45.
[4] Jain IP. Hydrogen the fuel for 21st century. Int J Hydrogen Energy 2009;34(17):7368–78.
[5] Wan W, et al. Adsorption, dissociation, and spillover of hydrogen over Au/TiO2 catalysts: the effects of cluster size and metal–support interaction from DFT. J Phys Chem C 2018;122(31):17895–916.
[6] Abe JO, et al. Hydrogen energy, economy and storage: review and recommendation. Int J Hydrogen Energy 2019;44(29):15072–86.
[7] Nakamura I, et al. Active sites for hydrogen dissociation over TiO x/Au (111) surfaces. J Phys Chem C 2011;115(32):16074–80.
[8] Beheshtian J, Ahmadi Peyghan A, Bagheri Z. Hydrogen dissociation on diene-functionalized carbon nanotubes. J Mol Model 2013;19(1):255–61.
[9] Pozzo M, Alfe D. Hydrogen dissociation and diffusion on transition metal (= Ti, Zr, V, Fe, Ru, Co, Rh, Ni, Pd, Cu, Ag)-doped Mg (0001) surfaces. Int J Hydrogen Energy 2009;34(4):1922–30.
[10] Xiao M, et al. Engineering energy level of metal center: Ru single-atom site for efficient and durable oxygen reduction catalysis. J Am Chem Soc 2019;141(50):19800–6.
[11] Liu X, et al. Defect stabilized gold atoms on graphene as potential catalysts for ethylene epoxidation: a first-principles investigation. Catal Sci Technol 2016;6(6):1632–41.
[12] Guo Y, Lang R, Qiao B. Highlights of major progress on single-atom catalysis in 2017. Catalysts 2019;9(2):135.
[13] Qiao B, et al. Single-atom catalysis of CO oxidation using Pt1/FeOx. Nat Chem 2011;3(8):634–41.
[14] Ghosh TK, Nair NN. Rh1/γ-Al2O3 single-atom catalysis of O2 activation and CO oxidation: mechanism, effects of hydration, oxidation state, and cluster size. ChemCatChem 2013;5(7):1811–21.
[15] Yang Z, Brady MP. Materials in clean power systems: applications, status and challenges. Int J Hydrogen Energy 2007;32(16):3610–796.
[16] Adams BD, Chen A. The role of palladium in a hydrogen economy. Mater Today 2011;14(6):282–9.
[17] Prabhukhot Prachi R, Wagh Mahesh M, Gangal Aneesh C. A review on solid state hydrogen storage material. Adv Energy Power 2016;4(2):11–22.
[18] Sahaym U, Norton MG. Advances in the application of nanotechnology in enabling a 'hydrogen economy'. J Mater Sci 2008;43(16):5395–429.
[19] Parkinson GS. Single-atom catalysis: how structure influences catalytic performance. Catal Lett 2019;149(5):1137–46.
[20] Cheng N, et al. Single-atom catalysts: from design to application. Electrochemical Energy Reviews 2019;2(4):539–73.
[21] Liang J-X, et al. Theoretical investigations of non-noble metal single-atom catalysis: Ni 1/FeO x for CO oxidation. Catal Sci Technol 2016;6(18):6886–92.
[22] Liu P, et al. Hollow engineering to Co@ N-doped carbon nanocages via synergistic protecting-etching strategy for ultrahigh microwave absorption. Adv Funct Mater 2021;31(27):2102812.
[23] Liang S, Hao C, Shi Y. The power of single-atom catalysis. ChemCatChem 2015;7:2559–67.
[24] Chen F, et al. Single-atom catalysis: bridging the homo-and heterogeneous catalysis. Chin J Catal 2018;39(5):893–8.
[25] Yan H, et al. Understanding the underlying mechanism of improved selectivity in pd1 single-atom catalyzed hydrogenation reaction. J Catal 2018;366:70–9.
[26] Xia Z, et al. Novel 2D Zn-porphyrin metal organic frameworks revived CdS for photocatalysis of hydrogen production. Int J Hydrogen Energy 2022;47(27):13340–50.
[27] Jaryal R, Kumar R, Khullar S. Mixed metal-metal organic frameworks (MM-MOFs) and their use as efficient photocatalysts for hydrogen evolution from water splitting reactions. Coord Chem Rev 2022;464:214542.
[28] Bonab SSY, et al. Assessment of the effect of electrophoretic deposition parameters on hydrogen storage performance of graphene oxide layer applied on nickel foam. Int J Hydrogen Energy 2022;47(4):2491–9.
[29] Verma SK, Shaz MA, Yadav TP. Enhanced hydrogen absorption and desorption properties of MgH2 with graphene and vanadium disulfide. Int J Hydrogen Energy 2022. https://doi.org/10.1016/j.ijhydene.2022.03.232.
[30] Mahamiya V, et al. High-capacity reversible hydrogen storage in scandium decorated holey graphyne: theoretical perspectives. Int J Hydrogen Energy 2022;47(12):7870–83.
[31] Hayat A, et al. Graphitic carbon nitride (g–C3N4)–based semiconductor as a beneficial candidate in photocatalysis diversity. Int J Hydrogen Energy 2022;47(8):5142–91.
[32] Kapoor A, Rajput JK. Nanostructured materials for the visible-light driven hydrogen evolution by water splitting: a review. Int J Hydrogen Energy 2022;47(40):17544–82.

[33] Noreen S, et al. Emerging 2D-Nanostructured materials for electrochemical and sensing Application-A review. Int J Hydrogen Energy 2022;47(2):1371–89.
[34] Shafiq F, et al. The construction of a highly efficient pn heterojunction Bi2O3/BiVO4 for hydrogen evolution through solar water splitting. Int J Hydrogen Energy 2022;47(7):4594–600.
[35] Shah AB, et al. Remarkable single atom catalyst of transition metal (Fe, Co & Ni) doped on C2N surface for hydrogen dissociation reaction. Nanomaterials 2023;13(1):29.
[36] Kumar P, et al. MXenes: emerging 2D materials for hydrogen storage. Nano Energy 2021;85:105989.
[37] Faye O, et al. Two-dimensional carbon nitride (C3N) nanosheets as promising materials for H2S and NH3 elimination: a computational approach. Phys E Low-dimens Syst Nanostruct 2020;117:113794.
[38] Guo J-H, et al. Pt4, Pd4, Ni4, and Ti4 catalyzed hydrogen spillover on penta-graphene for hydrogen storage: the first-principles and kinetic Monte Carlo study. Int J Hydrogen Energy 2018;43(4):2247–55.
[39] Lyu J, Kudiiarov V, Lider A. An overview of the recent progress in modifications of carbon nanotubes for hydrogen adsorption. Nanomaterials 2020;10(2):255.
[40] Dou B, et al. Hydrogen sorption and desorption behaviors of Mg-Ni-Cu doped carbon nanotubes at high temperature. Energy 2019;167:1097–106.
[41] Sharma V, et al. Hydrogen adsorption on pristine and platinum decorated graphene quantum dot: a first principle study. Int J Hydrogen Energy 2020;45(44):23977–87.
[42] Tierney HL, et al. Hydrogen dissociation and spillover on individual isolated palladium atoms. Phys Rev Lett 2009;103(24):246102.
[43] Slanina Z, et al. Geometrical and thermodynamic approaches to the relative stabilities of fullerene isomers. 2001.
[44] Khamatgalimov AR, Kovalenko VI. Substructural approach for assessing the stability of higher fullerenes. Int J Mol Sci 2021;22(7):3760.
[45] Fan M-F, Lin Z, Yang S. Closed-shell electronic requirements for small fullerene cage structures. J Mol Struct: THEOCHEM 1995;337(3):231–40.
[46] An W, et al. Ab initio calculation of carbon clusters. II. Relative stabilities of fullerene and nonfullerene C 24. J Chem Phys 2008;128(8):084301.
[47] Jensen F, Koch H. C 24: ring or fullerene? J Chem Phys 1998;108(8):3213–7.
[48] Chen Z, et al. Theoretical investigation into structures and magnetic properties of smaller fullerenes and their heteroanalogues. Theor Chem Acc 2001;106(5):352–63.
[49] Jensen F, Toftlund H. Structure and stability of C24 and B12N12 isomers. Chem Phys Lett 1993;201(1–4):89–96.
[50] Frisch, M., et al., 01; Gaussian, inc. Wallingford, CT, 2009.
[51] Tahir H, et al. Outstanding NLO response of thermodynamically stable single and multiple alkaline earth metals doped C20 fullerene. J Mol Liq 2020;305:112875.
[52] Ahmadi R, Pourkarim S. Investigation of fullerene (C. Int J Bio-Inorg Hybrid Nanomater 2015;4(4):249–54.
[53] Osuna S, Swart M, Sola M. Dispersion corrections essential for the study of chemical reactivity in fullerenes. J Phys Chem 2011;115(15):3491–6.
[54] Ignat'ev V, et al. Hydrogen bonds formed upon encapsulation of doxorubicin into amphiphilic N-vinylpyrrolidone copolymer: a quantum chemical study. Russ Chem Bull 2021;70(7):1269–74.
[55] Mukhtar A, Sarfaraz S, Ayub K. Organic transformations in the confined space of porous organic cage CC2; catalysis or inhibition. RSC Adv 2022;12(37):24397–411.
[56] Ren Q, et al. Density functional theory study of the mechanisms of iron-catalyzed cross-coupling reactions of Alkyl Grignard reagents. J Phys Chem 2013;117(4):756–64.
[57] Zhu C, Xia H. Carbolong chemistry: a story of carbon chain ligands and transition metals. Acc Chem Res 2018;51(7):1691–700.
[58] Soltani A, et al. Interaction of hydrogen with Pd-and co-decorated C24 fullerenes: density functional theory study. Synth Met 2017;234:1–8.
[59] Wang X, Liew KM. Density functional study of interaction of lithium with pristine and Stone-Wales-defective single-walled silicon carbide nanotubes. J Phys Chem C 2012;116(51):26888–97.
[60] Javan MB, et al. Adsorption and dissociation of H2 on Pd doped graphene-like SiC sheet. Int J Hydrogen Energy 2016;41(48):22886–98.
[61] Wu H, Fan X, Kuo J-L. Metal free hydrogenation reaction on carbon doped boron nitride fullerene: a DFT study on the kinetic issue. Int J Hydrogen Energy 2012;37(19):14336–42.
[62] Mahamiya V, Shukla A, Chakraborty B. Scandium decorated C24 fullerene as high capacity reversible hydrogen storage material: insights from density functional theory simulations. Appl Surf Sci 2022;573:151389.
[63] Righi G, Magri R, Selloni A. H2 dissociation on noble metal single atom catalysts adsorbed on and doped into CeO2 (111). J Phys Chem C 2019;123(15):9875–83.
[64] Vayner G, et al. Steric retardation of SN2 reactions in the gas phase and solution. J Am Chem Soc 2004;126(29):9054–8.
[65] Venkataramanan NS, Suvitha A, Kawazoe Y. Unravelling the nature of binding of cubane and substituted cubanes within cucurbiturils: a DFT and NCI study. J Mol Liq 2018;260:18–29.
[66] Lu T, Chen F. Multiwfn: a multifunctional wavefunction analyzer. J Comput Chem 2012;33(5):580–92.
[67] Humphrey W, Dalke A, Schulten K. VMD: visual molecular dynamics. J Mol Graph 1996;14(1):33–8.
[68] Aireddy DR, Ding K. Heterolytic dissociation of H2 in heterogeneous catalysis. ACS Catal 2022;12(8):4707–23.